A New Generation of Light Scattering Device with Real Time Data Analysis for Rheo-optical Measurements

Deepak Arora[1]*, Souvik Nandi[2], H. Henning Winter[1,2]*

[1]Department of Polymer Science and Engineering and [2]Department of Chemical Engineering, University of Massachusetts Amherst, Amherst, MA 01003, USA

* Corresponding author: winter@ecs.umass.edu, deepakarora04@gmail.com
Fax: x1.413.545.1647

Received: 22.3.2011, Final version: 7.6.2011

Abstract:
An apparatus for small angle light scattering (SALS) and light transmission measurements under shear was built and tested at the University of Massachusetts Amherst. As a new development, the polarization direction can be rotated by a liquid crystal polarization rotator (LCPR) with a short response time of about 20 ms. The experiments were controlled and analyzed with a LabVIEW™ based code (LabVIEW™ 7.1) in real time. Quiescent and flow-induced crystallization experiments on isotactic poly-1-butene (iPB) were conducted to demonstrate the instrument and software capabilities. Software was designed with a modular approach, so that further modules can be added to investigate other systems such as polymer blends, colloidal suspensions, solutions with droplets etc. A replica of the SALS apparatus was custom built for ExxonMobil Research in Clinton NJ.

Zusammenfassung:
Eine Apparatur für Kleinwinkellichtstreuung (SALS) und Lichttransmissionsmessungen in Scherung wurde an der University of Massachusetts Amherst entwickelt und getestet. Eine neue Entwicklung stellt die Drehung der Polarisationsrichtung durch einen flüssigkristallinen Polarisationsrotator (LCPR) mit einer kurzen Antwortzeit von 20 ms dar. Die Experimente wurden mit Hilfe einer LabView™-Steuerung kontrolliert und in Echtzeit analysiert (LabView™ 7.1). Kristallisationsexperimente ohne und in Strömung wurden an isotaktischem Poly-1-Buten (iPB) durchgeführt, um die Möglichkeiten der Apparatur und der Software darzulegen. Die Softwaresteuerung ist modular aufgebaut, so dass weitere Module hinzugefügt werden können, um andere Systeme (z. B. Polymerblends, kolloidale Suspensionen, Lösungen mit Tröpfchen etc.) zu untersuchen. Die SALS-Apparatur wurde für ExxonMobil Research in Clinton (NJ) konstruiert.

Résumé:
Un appareil pour des mesures de diffusion de la lumière aux petits angles (SALS) et de transmission de la lumière sous écoulement a été construit et testé à l'université de Massachusetts Amherst. En termes de nouveau développement, la direction de la polarisation peut être tournée grâce à un modulateur de polarisation cristal liquide (LCPR) qui possède un temps de réponse court de 20 ms. Les expériences ont été contrôlées et analisées avec un code LabVIEW™ (LabVIEW™ 7.1) en temps reel. Des expériences de cristallisation au repos et induites par l'écoulement ont été menées avec un poly-1-butène isotactique (iPB) afin de démontrer les possibilités de l'instrument et du programme informatique. Le programme a été conçu avec une approche modulaire, de telle sorte que de futures modules peuvent être additionnés afin d'étudier d'autres systèmes comme les mélanges de polymères, les suspensions colloïdales, les solutions contenant des gouttelettes, etc. L'appareil de SALS a été spécialement construit pour ExxonMobil Research à Clinton NJ

Key words: rheology, light scattering, transmission intensity measurements, liquid crystal polarization rotator

1 INTRODUCTION

Small angle light scattering (SALS) is gaining ample popularity in material industries as a preferred technique to perform real time structural analysis especially as a combinatorial tool with rheometry [1–5]. The fast data acquisition, easy handling, robustness and the ease of integrating with variety of other techniques such as X-ray, optical microscopy (OM) and differential scanning calorimetry (DSC) make SALS an attractive sensor [6, 7] even for incorporating with industrial film extruders and injection molding machines. Here we present a house-built device that can perform light scattering and transmission intensity measurements simultaneously while analyzing the data in real time. The device grew out of an earlier apparatus at the University of Massachusetts Amherst [8, 9] and incorporated a liquid crystal based device to control the polarization direction of a linearly polarized laser beam. Crystal-

DOI: 10.3933/ApplRheol-21-42633

lization of isotactic poly-1-butene with and without flow was studied to validate the device [10, 11]. The material response for polarized light was captured under cross and parallel polars while unpolarized light did not provide any characteristic scattering for polyethylene films.

In their seminal work in light scattering of polymers, Stein and coworkers laid the theoretical foundation for relating structure to the measured SALS [12]. The analysis was further extended to polymer films with orientation fluctuations [13], random assembly of truncated spherulites [14] and oriented films [15]. The Stein-Wilson theory provides the light scattering invariants for random orientation correlations [16].

$$Q_\delta = \int_{q_1}^{q_2} I_{HV}(q) q^2 dq \propto \langle \delta^2 \rangle$$

$$Q_\eta = \int_{q_1}^{q_2} \left(I_{VV}(q) - \frac{4}{3} I_{HV}(q) \right) q^2 dq \propto \langle \eta^2 \rangle$$

$$q = \frac{4\pi}{\lambda} \sin\frac{\theta}{2} \qquad (1)$$

Q_δ, Q_η, q, δ, η, θ, and λ are the orientation fluctuation invariant, density fluctuation invariant, wave vector, orientation fluctuations, density fluctuations, scattering angle and wavelength of the light source, respectively. These invariants are the measure of mean square fluctuations. Mean square density fluctuations, $\langle \eta^2 \rangle$, are related to the volume fraction of anisotropic aggregates, ϕ_A, as

$$\langle \eta^2 \rangle = \phi_A (1 - \phi_A) (\bar{\alpha}_A - \alpha_s)^2 \qquad (2)$$

$\bar{\alpha}_A$ and α_s are the average polarizability of the aggregate and the surrounding, respectively. For a crystallizing polymer, spherulites can be treated as anisotropic aggregates of crystals in an isotropic melt. Mean square orientation fluctuations, $\langle \delta^2 \rangle$, offer an estimate of the crystal volume fraction in the sample.

$$\langle \delta^2 \rangle = \phi_A \delta_A^{\,2} + (1 - \phi_A) \delta_s^{\,2} \qquad (3)$$

δ_A and δ_s define the anisotropy of the aggregate and surrounding, respectively. For a melt, δ_s can be assumed to be zero. For semicrystalline aggregates, their anisotropy can be expressed as a function of their crystal content (Equation 4).

$$\delta_A = \phi_{cry,A} \delta^o_{cry} f_{cry,A} + (1 - \phi_{cry,A}) \delta^o_{amo} f_{amo,A} + \delta_F \qquad (4)$$

$\phi_{cry,A}$, δ^o_{cry}, δ^o_{amo}, δ_f, $f_{cry,A}$, and $f_{amo,A}$, are the volume fraction of the crystal in the aggregate, intrinsic anisotropy of the crystal, anisotropy of the amorphous region, form anisotropy, orientation function for the crystals in aggregate and orientation function for the amorphous regions in the aggregate, respectively. The assumptions are that all crystals reside within the aggregates

$$\phi_{cry} = \phi_A \phi_{cry,A} \qquad (5)$$

that form and amorphous anisotropies can be neglected. Then, Equations 3, 4, and 5 combined predict the mean square anisotropy for a volume-filling sample

$$\langle \delta^2 \rangle = \phi_{cry}^{\,2} \delta^{o\,2}_{cry} f_{cry,A}^{\,2} \propto Q_\delta \qquad (6)$$

The crystal volume fraction in the sample is predicted to be proportional to the square root of the mean square orientation fluctuation invariant

$$\phi_{cry}(t) \propto \sqrt{Q_\delta(t)} \qquad (7)$$

under the assumption that δ^o_{cry} and $f_{cry,A}$ remain constant during crystallization. The transmission intensity under parallel-polars (I_{HH}) defines the evolving turbidity, $\mu = -(1/h)\ln(I_{HH}/I_o)$, of the sample due to crystallization. h and I_o are sample thickness and laser source intensity, respectively [8, 17].

2 INSTRUMENT DESCRIPTION

In the SALS experiment, linearly polarized light from a 5 mW He-Ne laser (632.8 nm wave length) passes through a linear polarizer followed by a beam splitter where the source intensity, I_o, is measured by a photodiode (Figure 1). The transmitted beam then passes through a liquid crystal polarization rotator (LCPR). The polymer sample, held in a shearing device, is placed in the path of the polarized light to obtain the scattering pattern. Scattered light from the polymer sample generates an image on a polarizing screen under

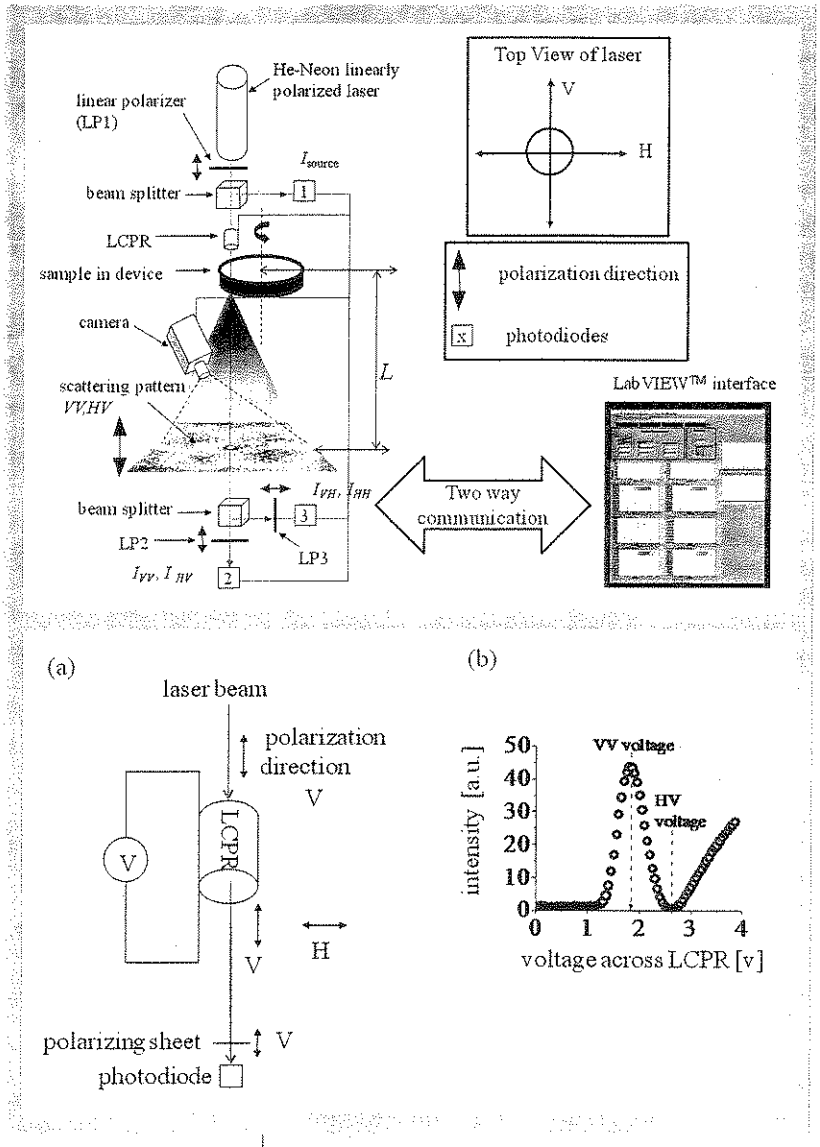

Figure 1 (above): Schematic for the small angle light scattering device. Transmission measurements are performed along with scattering measurements. Double sided arrows represent the direction of polarization.

Figure 2: (a) Working principle of LCPR. A dedicated low voltage controller applies different voltages across the LCPR and the intensity of the output beam is measured using a photodiode. (b) A characteristic LCPR curve. Maximum and the minimum intensities correspond to the voltages for VV and HV scattering.

a CCD camera. HV and VV patterns are recorded, digitized, and analyzed during the experiment. The scattering patterns are corrected for image distortions, which arise from the distance and angle of the camera. The main beam of the transmitted light passes through the center hole in the screen and gets split for cross polar and parallel polar transmission intensity measurements. The experimental set-up is shown in Figure 1. Its components are:

- A 5 mW linearly polarized Helium-Neon (He-Ne) laser is held vertically on an optical bench that passes through a linear polarizer followed by a beam splitter. The polarization of the laser beam and the linear polarizer are inside-out and are termed as V (Vertical). The beam diameter is ≈ 1mm.
- About half of the beam is used to measure the source intensity in order to track the fluctuations in laser intensity and the other half is transmitted through the beam splitter for scattering and further transmission measurements.
- For control of the polarization direction, the beam passes through a liquid-crystal polarization rotator (LCPR) driven by a dedicated low-voltage controller. Depending on the applied voltage across the LCPR, the incoming linearly polarized beam can be rotated by a fixed angle from 0 to 180°.
- A sample holder is placed on the bench that can be moved vertically to change the scattering angle range and the distance between sample and screen (L).
- A polarization screen (analyzer) with an opaque background is placed below the sample holder to obtain the scattered image. The analyzer has the same polarization as the source i.e. V. The analyzing screen has a hole in the center to measure transmitted intensities.
- A CCD camera is placed at an angle above the polarization screen to capture the images. CCD camera is placed on a different optical bench in order to keep the optical alignment undisturbed from the camera adjustments.
- A beam splitter is placed below the analyzing screen and two photodiodes measure the transmitted intensities at orthogonal polarization directions simultaneously. The photodiode 2 and photodiode 3 have linear polarizers in front of them with V and H orientations, respectively.

2.1 LIQUID CRYSTAL POLARIZATION ROTATOR (LCPR)

The LCPR device (meadowlark optics) is designed for an input wavelength of 632.8 nm. It combines a liquid crystal variable retarder with a zero-order polymer quarter wave retarder. It can rotate the polarization direction of the incoming monochromatic linearly polarized beam from 0 to 180° depending on the applied voltage. The retarder material is a birefringent nematic liquid crystal polymer which is sandwiched between two optically flat fused silica windows coated with transparent indium tin oxide (ITO). The working principle of the device is explained in Figure 2. The incoming laser beam to the LCPR is linearly polarized with a polarization of V. The polarization direction of the output beam changes as different voltages are applied in the increments of 0.01 volts across the LCPR. The voltage increment and the range of applied voltage are controlled via a

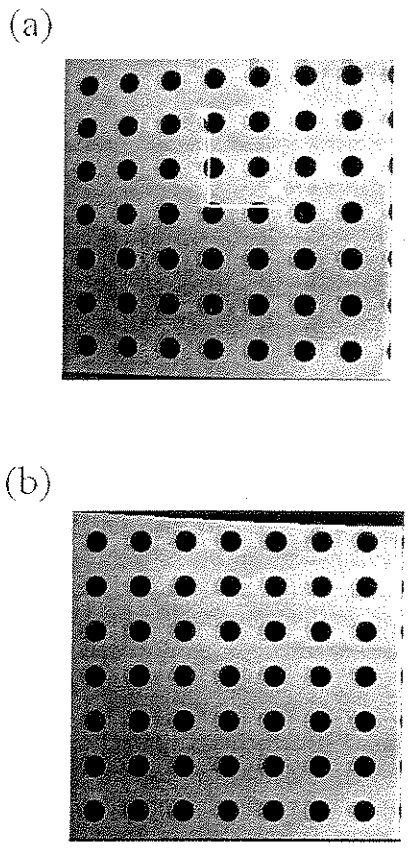

LabVIEW™ written code. The changed state of polarization is detected using a photodiode with a linear polarizer (V) in front of it (Figure 2a). If the polarization direction of the output beam is same as input i.e. V, then the photodiode measures maximum intensity and provides us a voltage necessary for 0° rotation of input beam. The intensity measured by the photodiode is minimum (close to zero) for a rotation of 90° (Figure 2b). The schematic shown in Figure 2a is a part of the whole light scattering train (Figure 1). The intensities measured by the photodiodes are normalized by the source intensity to correct for the fluctuating laser intensity.

2.2 NOMENCLATURE FOR SCATTERING IMAGES AND TRANSMISSION INTENSITIES

The polarization direction for the analyzing screen and the source is chosen to be always V. When the leaving beam from LCPR has same polarization direction as the source and the analyzing screen i.e. V, we obtain a VV scattering pattern with transmission intensities being VV (photodiode 2) and VH (photodiode 3). When the leaving beam has a polarization direction of H, we get a HV scattering pattern with transmission intensities being HV (photodiode 2) and HH (photodiode 3).

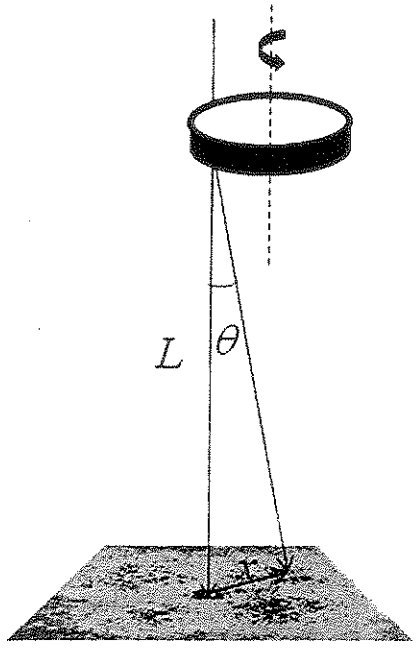

Figure 3 (left): Image correction for CCD camera tilt: An image with equally spaced circular dots was printed on a piece of paper and was used as a template to correct for the image distortion from camera angle and distance (a) image captured from the CCD camera before correction shows distorted circular dots. The distortion is along the X-axis as well as the Y-axis. (b) Corrected image after applying the necessary mathematical scheme.

Figure 4: Scattering wave vector, q, calculation: Scattering angle from camera length L and distance of a point on the scattering image, x.

2.3 IMAGE CORRECTION FOR CCD CAMERA TILT

The analyzing screen for the SALS images is aligned normal to the incident beam while the detector, a charge-coupled device (CCD) camera, records these images at an angle to the analyzing screen (Figure 1). The angular position of the CCD results in perspective distortion of the captured images. An example of such distortion is shown in Figure 3a. For Calibration, a reference image with a regular pattern of equal size circular dots was placed on the screen and its image was taken using the CCD camera. The laser was switched off for this part of the experiment and a white light source was used to illuminate the pattern. The captured image (Figure 3a) shows dots that are distorted from their true shape. The image was then corrected using a mathematical scheme in LabVIEW™ (Figure 3b). The correction parameters were saved and used for following SALS experiments.

2.4 SCATTERING WAVE VECTOR (Q) CALCULATIONS

The momentum change upon elastic scattering is described by the wave vector, q, which is related to the length scales, d, that scatter light of wavelength, λ at scattering angle of θ (Figure 4). The wave vector is given as $q = (4\pi/\lambda)\sin(\theta/2) = 2\pi/d$. The Scattering angle depends on the camera length, L, the distance between sample and analyzing screen, and the distance of an image point from the center of the screen, x, as $\tan\theta = x/L$. The q-range can be altered by varying L or the size of the screen.

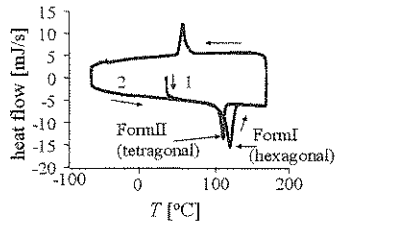

1 – first heating cycle
2 – second heating cycle

T_{m-I}=120.0 °C (100-130 °C)
T_{m-II}=110.7 °C (100-120 °C)
T_c=54.7 °C (70-50 °C) at 10 K/min

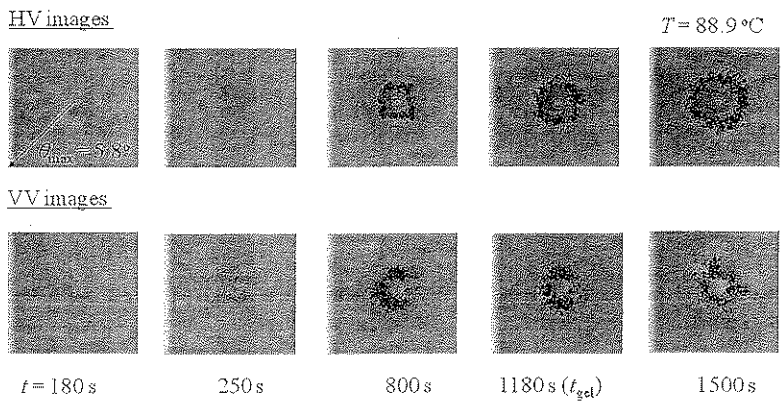

Figure 5 (left): Differential scanning calorimetry for iPB for heating and cooling rates of 10 K/min. Two polymorphs of iPB, FormI and FormII, were observed during first and second heating, respectively.

Figure 6: Small angle light scattering (SALS) images under cross-polars and parallel-polars for crystallizing isotactic poly-1-butene at 88.9°C. Crystallization was performed without applying any flow.

2.5 SOFTWARE FOR REAL TIME DATA ACQUISITION AND ANALYSIS

The input parameters to the SALS analysis software are the sample distance from the analyzing screen (L), angle of analyzing screen, Image size in pixels, HV and VV voltages to the LCPR, number of samples and sampling interval. The tilt angle for analyzing screen was zero for the experimental data presented in Figures 6, 7 and 8. Users can add multiple images for HV and VV patterns to improve the signal quality for slowly varying structures. Software combines source intensity (photodiode1) and transmission intensities (photodiodes 2 and 3) measurements and calculates the light scattering invariants in real time. Line integrals (1-Dimentional) as well as areal integrals (2-Dimentional) are obtained by analyzing HV and VV patterns in real time according to Equation 1. For the line integrals, user can control the initial and final pixel coordinates of a line during the experiments and can precisely center it with the acquired images. Intensity, I, versus q and Iq^2 versus q curves are also plotted in real time during the experiment.

3 EXAMPLE: CRYSTALLIZATION OF ISOTACTIC POLY-1-BUTENE

3.1 MATERIAL AND SAMPLE PREPARATION

Isotactic poly-1-butene (iPB), from Basell, with M_w = 176000 and M_w/M_n of 5.7, served as test material. Pellets of iPB (as obtained from Basell) were compression molded into thick sheets, from which samples were cut for Differential Scanning Calorimetry (DSC) and optical measurements. The iPB was used without a nucleating agent. Differential scanning calorimetry (DSC) was carried out under nitrogen in a DSC Q1000 (TA Instruments) using standard aluminum pans (from TA instruments) 6 mm in diameter and weighing about 24 mg. A thin sample (about 12 mg) was pressed into a DSC pan and heated above melting temperature to establish uniform contact between polymer and pan. For the DSC measurements, samples were heated as well as cooled at 10K/min. First melting, second melting, and crystallization peaks were observed at 120°C (100–130°C), 110°C (100–120°C), and 54°C, respectively (Figure 5). First melting belongs to the crystal FormI of iPB, which has a density of 950 Kg/m^3 and is a thermodynamically stable form. Second melting belongs to FormII that is less dense (907 Kg/m^3) than FormI and is a kinetically favored crystal form. FormII transforms into FormI within 7-12 days at room temperature and atmospheric pressure [18 – 21].

3.2 TEMPERATURE AND SHEARING PROTOCOL

For all experiments, samples were heated to 174°C, kept there for about 15 minutes. Such a high temperature (about 50 K above melting) was used to erase the thermo-mechanical history and to melt all the crystallites present in the sample as recommended by Hadinata et al. [22]. Then the sample was cooled down to T_x, the temperature for isothermal crystallization. Time t = 0 was assigned to the instant at which the experimental temperature T_x was reached. Sample was sheared for a duration of t_s from t = 0 and then crystallized isothermally without any further shearing. Cooling was performed fast enough to avoid any crystallization during cooling. The main purpose of adopting Janeschitz-Kriegl protocol [23, 24] was to isolate shearing action from crystal growth. This way dynamics of flow was governed by the melt dynamics instead of suspension dynamics (solid crystal suspended in melt).

3.3 QUIESCENT CRYTSTALLIZATION OF IPB

The development of four-clover light scattering patterns (HV images), a characteristic of spherulitic morphology, is presented in Figure 6. Crys-

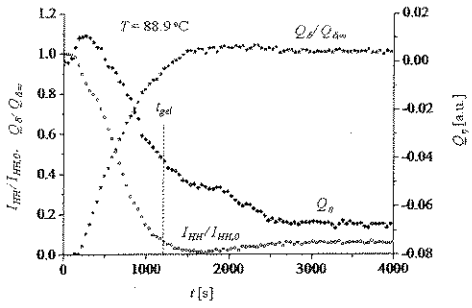

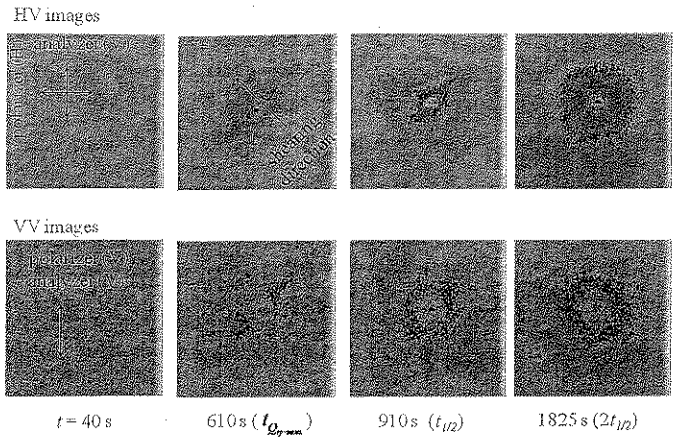

Figure 7 (left):
SALS and transmission measurements for crystallizing isotactic poly-1-butene at 88.9°C. Invariants were obtained by analyzing the images in Figure 6.

Figure 8:
Cross-polar (HV) and parallel-polar (VV) images from SALS during crystallization of iPB at 98.9°C after shearing with $\dot{\gamma}$ = 7 s^{-1} for 30 s.

tallization was performed isothermally at 88.9°C without any preshear. The maximum scattering angle was 5.8°, corresponding to a maximum q value of 1 μm^{-1} and the minimum length scale of 6.3 μm. Scattering images under parallel-polars are shown as well. Images are corrected for the excess scattering (due to melt and stage windows) as well as the fluctuations in source intensity. Light scattering invariants were calculated according to the areal integrals of Equation 1. The measured density fluctuation invariant goes through a maximum at about t = 250 – 400 s for six different measurements (Figure 7). For a system consisting of anisotropic scatterers in an isotropic matrix with random orientation fluctuations, this maximum characterizes the instant when half of the sample volume is occupied by the scattering aggregates [16]. The normalized orientation fluctuation invariant ($Q_\delta(t)/Q_{\delta-\infty}$) grows with time and reaches a steady value within about 1600-2400 s. Due to growing inhomogeneities, the normalized parallel polar transmission intensity ($I_{HH}(t)/I_{HH-\infty}$) decreases and reaches a plateau in about 1600 – 1700 s. The HV pattern loses its four clover shape and becomes isotropic after this.

3.4 SHEAR-INDUCED CRYSTALLIZATION OF IPB

Figure 8 shows a set of SALS images under cross-polars (HV) and parallel-polars (VV) modes for crystallization of iPB at 98.9°C with $\dot{\gamma}$ = 7 s^{-1} and strain units of 210. The sample reached a temperature of 98.9°C (T_x) at t = 0 and was sheared for a duration of 30 s. Shearing direction was at 45° to both polarizer and analyzer, and is shown in Figure 8. Light scattering images just after shearing, t^+_s, showed very little scattering. An anisotropic scattering pattern, perpendicular to the flow direction, was observed at 610 s under cross-polars. Scattering in the direction perpendicular to the flow corresponds to the development of oriented shish-like structure in the flow direction. VV image at this time also had anisotropic scattering perpendicular to the flow, though the development of shish-type structures was more clearly visible under HV mode of scattering. HV images showed the enhanced scattering in the flow direction at the later stages and a transformation from anisotropic scattering to isotropic scattering. Enhanced scattering in the flow direction is attributed to structure growth perpendicular to the flow. It was attributed to the lamellar kebab growth on the existing shish. Crystallization in the absence of flow would give rise to spherulitic growth in the relaxed melt, which would lead to isotropic scattering.

4 LINEAR RHEOMETER WITH AN INVERTED LIGHT SCATTERING SET-UP

The SALS apparatus described above has a vertical configuration with the laser source being at the top. The similar set-up has been combined with a house-built linear parallel plate rheometer and a customized optical microscope (Figure 7). A program is being developed in LabVIEW™ to synchronize rheometry with image acquisition in optical microscopy and SALS.

5 DISCUSSION

These optical measurements provide us with a few time scales that can serve as characteristic times for crystallization. These include the characteristic times from orientation fluctuation invariants, from the maximum of density fluctuations invariants and transmission intensity measurements. Maximum in density fluctuation invariant corresponds to a sample which is half filled with aggregates according to the Stein-Wilson theory [16]. We do not observe this in our experiments though. A detailed experimental study will be the part of future publications. Scattering images can also be used to follow the size of growing entities such as spherulites and shish-kebab structures.

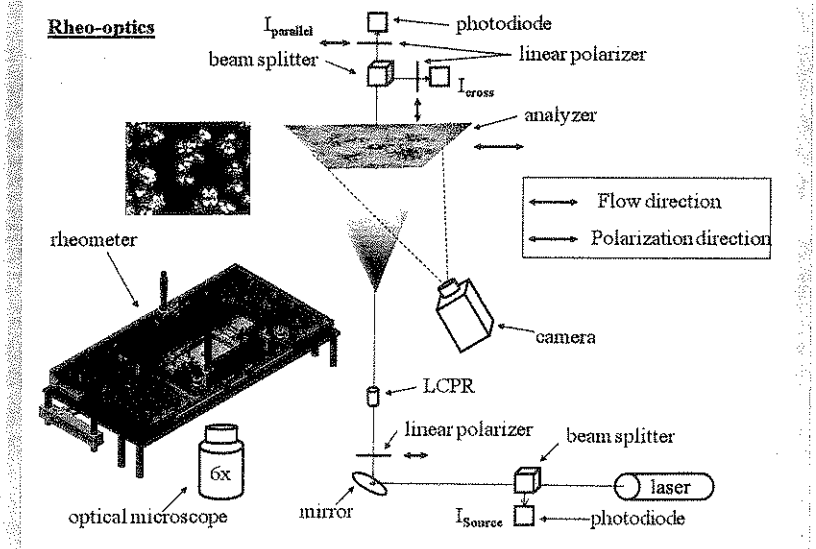

Figure 9:
An inverted SALS set-up combined with a rheometer and an optical microscope to follow the evolution of mechanical and optical properties simultaneously along with the morphology from scattering and optical microscopy images.

6 CONCLUSIONS

The device at UMass Amherst was developed to investigate the crystallization of thermoplastic semicrystalline polymers though it can readily be extended to polymer blends, concentrated suspensions, micellar solutions, crude oil and to variety of other materials [1, 25–28]. A LabVIEW™ based platform provides flexibility to add new modules to the existing code. The house-built small angle light scattering apparatus is able to perform following in real time:

- Transmission intensity measurements under cross and parallel polars
- Record scattering images under cross and parallel polars and their real time analysis to obtain light scattering invariants
- Source intensity measurements
- Controlling polarization direction using a liquid crystal based device for fast response time

As a novel addition a liquid crystal based device is incorporated as a superior substitute of quarter wave plate to control the polarization direction of a linearly polarized laser. The LCPR unit not only provides faster rotation of light but also is less bulky than the traditional quarter wave plate set-up which requires a motor to rotate the plate. The set-up is being combined with a rheometer and an optical microscope.

ACKNOWLEDGMENTS

We are grateful for the funding under NSF grant. G.G.Fuller helped with the selection of the LCPR.

REFERENCES

[1] Elmoumni A, Franck AJ, Helgeson ME, Reichert MD, McMullan JM, Wagner NJ: Simultaneous light scattering-rheology measurements for studying stress induced phase transitions, 15th International Congress on Rheology/80th Annual Meeting of the Society-of-Rheology (2008) 1147 – 1149.

[2] Lauger J, Gronski W: A melt rheometer with integrated small-angle light-scattering, Rheol. Acta 34 (1995) 70-79.

[3] Hou YY, Kassim HO: Instrument techniques for rheometry, Rev. Sci. Inst. 76 (2005) 1-19.

[4] Acierno S, Palomba B, Winter HH, Grizzuti N: Effect of molecular weight on the flow-induced crystallization of isotactic poly(1-butene), Rheol. Acta 42 (2003) 243– 250.

[5] Klein C, Venema P, Sagis L, van Dusschoten D, Wilhelm M, Spiess HW, van der Linden E, Rogers SS, Donald AM: Optimized rheo-optical measurements using fast fourier transform and oversampling, Appl. Rheol. 17 (2007)

[6] Wutz C, Bark M, Cronauer J, Dohrmann R, Zachmann HG: Simultaneous measurements of small-angle x-ray-scattering, wide-angle x-ray-scattering, and light-scattering during phase-transitions in polymers, Rev. Sci. Inst. 66 (1995) 1303– 1307.

[7] Wurm A, Minakov AA, Schick C: Combining x-ray scattering with dielectric and calorimetric experiments for monitoring polymer crystallization, Europ. Poly. J. 45 (2009) 3280– 3289.

[8] Pogodina NV, Lavrenko VP, Srinivas S, Winter HH: Rheology and structure of isotactic polypropylene near the gel point: Quiescent and shear-induced crystallization, Polymer 42 (2001) 9031 – 9043.

[9] Pogodina NV, Siddiquee SK, van Egmond JW, Winter HH: Correlation of rheology and light scattering in isotactic polypropylene during early stages of crystallization, Macromol. 32 (1999) 1167– 1174.

[10] Arora D, Rothstein JP, Winter HH: Criteria for shear-induced crystallization: Strain and weissenberg number (Unpublished work).

[11] Arora D, Winter HH: Network formation in a semicrystalline polymer at the early crystallization stages: From nucleation to percolation (Unpublished work).

[12] Stein RS, Rhodes MB: Photographic light scattering by polyethylene films, J. Appl. Phys. 31 (1960) 1873 – 1884.

[13] Stein RS, Wilson PR: Scattering of light by polymer films possessing correlated orientation fluctuations, J. Appl. Phys. 33 (1962) 1914 – 1922.

[14] Stein RS, Chu W: Scattering of light by disordered spherulites, J. Polym. Sci. Part a-2-Poly.m Phys. 8 (1970) 1137 – 1157.

[15] Stein RS, Hashimoto.T: Scattering of light from oriented polymer films .2, J. Polym. Sci. Part a-2-Poly.m Phys. 8 (1970) 1503 – 1519.

[16] Koberstein J, Russell TP, Stein RS: Total integrated light-scattering intensity from polymeric

solids,J. Polym. Sci. Part a-2-Poly.m Phys. 17 (1979) 1719 – 1730.
[17] Elmoumni A, Gonzalez-Ruiz RA, Coughlin EB, Winter HH: Isotactic poly(propylene) crystallization: Role of small fractions of high or low molecular weight polymer, Macromol. Chem. Phys. 206 (2005) 125 – 134.
[18] Kalay G, Kalay CR: Structure and physical property relationships in processed polybutene-1, J. Appl. Polym. Sci. 88 (2003) 814 – 824.
[19] Kaszonyiova M, Rybnikar K, Geil PH: Polymorphism of isotactic poly(butene-1), J. Macromol. Sci.-Phys. B44 (2005) 377 – 396.
[20] Azzurri F, Gomez MA, Alfonso GC, Ellis G, Marco C: Time-resolved saxs/waxs studies of the polymorphic transformation of 1-butene/ethylene copolymers, Conference on Synchrotron Radiation in Polymer Science II (2002) 177 – 189.
[21] Azzurri F, Flores A, Alfonso GC, Calleja FJB: Polymorphism of isotactic poly(1-butene) as revealed by microindentation hardness. 1. Kinetics of the transformation, Macromol. 35 (2002) 9069 – 9073.
[22] Hadinata C, Gabriel C, Ruellman M, Laun HM: Comparison of shear-induced crystallization behavior of pb-1 samples with different molecular weight distribution, J. Rheol. 49 (2005) 327 – 349.
[23] Janeschitz-Kriegel H: Crystallization modalities in polymer melt procesing, Fundmental Aspects of Structure Formation, Springer, NewYork (2010).
[24] Janeschitz-Kriegl H: Phases of flow-induced crystallization of i-pp: How remote pieces of the puzzle appear to fit, Macromol. 39 (2006) 4448 – 4454.
[25] van Egmond JW, Werner DE, Fuller GG: Time-dependent small-angle light-scattering of shear-induced concentration fluctuations in polymer-solutions, J. Chem. Phys. 96 (1992) 7742 – 7757.
[26] Stein RS: Recent advances in rheo-optical studies of polymers in the solid-state, Polym. J. 17 (1985) 289 – 305.
[27] Versmold H: Scattering from shear-ordered dispersions, Appl. Rheol. 17 (2007) 11412 – 11418.
[28] Glass JE, Schulz DN, Zukoski CF: Polymers as rheology modifiers – an overview, ACS Symposium Series 462 (1991) 2 – 17.